Imaging coherent phonons and precursor dynamics in LaFeAsO with 4D ultrafast electron microscopy

Ryan A. Gnabasik, Pranav K. Suri, Jialiang Chen, and David J. Flannigan

Phys. Rev. Materials **6**, 024802 — Published 22 February 2022

DOI: 10.1103/PhysRevMaterials.6.024802

Imaging Coherent Phonons and Precursor Dynamics in LaFeAsO with 4D Ultrafast Electron Microscopy

Ryan A. Gnabasik[†§], Pranav K. Suri[†‡], Jialiang Chen, and David J. Flannigan[*]

Department of Chemical Engineering and Materials Science, University of Minnesota, Minneapolis, Minnesota 55455, United States

Abstract: We used 4D ultrafast electron microscopy (UEM) to directly image femtosecond photoinduced structural dynamics in single-crystal LaFeAsO at initial temperatures of 300 K and 100 K, above and below the known structural and magnetic phase transition temperatures, respectively. With nanometer-ps resolution, we resolved an initial (precursor) sigmoid-like response arising from photothermal expansion and lattice re-orientation that precedes the onset of propagating coherent acoustic phonons (CAPs). In the specific regions probed, the precursor response at 100 K is shorter than at 300 K ($t_{0.5;100\ K}$ = 11.3 ps *vs.* $t_{0.5;300\ K}$ = 17.8 ps), and the CAP oscillation frequency is lowered with cooling ($f_{CAP;100\ K}$ = 12 GHz *vs.* $f_{CAP;300\ K}$ = 21 GHz), correlated to known lattice softening due to the structural phase change. The transient CAP behaviors at 300 K are dispersive, displaying an exponentially decaying phase velocity over the first nanosecond. Further, the CAP symmetry at 300 K matches a first-order antisymmetric shear mode (A_1), while at 100 K it is best matched by a mostly non-dispersive zero-order symmetric mode (S_0). These findings illustrate the sensitivity of UEM imaging to spatially heterogeneous dynamics in the Fe-pnictide materials and more broadly in other quantum materials.

*Corresponding author:
Email: flan0076@umn.edu
Office: +1 612-625-3867

†These authors contributed equally to this work.

§Current address: Department of Mechanical Engineering, University of California, Santa Barbara

‡Current address: Micron Technology, Boise, ID

Numerous studies of superconducting materials and their parent compounds with ultrafast structural probes have led to increased understanding of the relationship between transient lattice distortions and superconductivity. The behaviors typically probed include electron-phonon coupling, phonon-mode coupling, and optical-phonon symmetries and lifetimes on femtosecond (fs) to picosecond (ps) timescales [1-17]. Indeed, such work has illuminated microscopic aspects of coupling and phonon-driven modulation of interatomic distances [2-7,10,11,14] and the roles of defects and the impact on phase-transition behaviors [1,8]. Unraveling interwoven dynamics thus enables non-equilibrium relationships between the structural and electronic sub-systems to be directly interrogated. Specifically with respect to the parent compounds of the Fe-pnictide superconductors, ultrafast X-ray and electron scattering, as well as ultrafast vibrational spectroscopies, have been used to probe the effects of coherent phonon excitation on distortion of the Fe-As unit, on electron-phonon coupling strength, on the interplay between spin and coherent optical phonons, and on the possible relationship between structural distortions and the nematic phase [18-24].

In addition to THz optical modes, low-energy GHz excitations in the form of coherent acoustic phonons (CAPs) have been linked to phase transitions and competing orders in Fe-pnictide compounds using ultrafast pump-probe spectroscopy [10,23,25-29]. Because key properties, including T_c and spatial inhomogeneities, are sensitive to strain [30-34], CAP behavior could potentially serve as an indicator of variations in stiffness and of precursors to charge/spin ordering and periodicity. Indeed, non-equilibrium temperature-dependent CAP behaviors and anomalies at transition temperatures (*e.g.*, for spin-density waves) have been observed in doped $CaFe_2As_2$ and doped and undoped $BaFe_2As_2$ with transient reflectivity [25,26,29]. Thus, owing to the propagating nature of fs photoexcited CAPs, real-space studies

may provide useful insights into the interplay between structure and morphology, strain waves, and lattice elastic properties associated with phase domains, boundaries, and transitions.

Real-space imaging with nanometer-ps resolution of fs photoexcited CAP dynamics has been demonstrated on a variety of materials with 4D ultrafast electron microscopy (UEM). By accessing real-space information, it has been shown that phonon nucleation occurs preferentially at lattice discontinuities and interfaces, and that specific behaviors are sensitively dependent upon nanoscale morphology [35-43]. Accordingly, here we used UEM bright-field imaging to study fs photoexcited CAP dynamics in undoped LaFeAsO at 300 K and at 100 K (*i.e.*, above and below the known structural and magnetic phase-transition temperatures) [44-47]. We were motivated to do this study by the general dearth of non-equilibrium studies on LaFeAsO and by the lack of any information pertaining to the *nanometer-ps spatiotemporal evolution* of CAP dynamics in Fe-pnictide compounds [48]. We also sought to explore the feasibility of using UEM imaging to correlate real-space CAP dynamics with the lattice softening and phase ordering behaviors that occur upon cooling [45].

MATERIALS AND METHODS

Specimen preparation and characterization. Crystals of undoped LaFeAsO were grown using a flux method [49]. Electron-transparent lamellae for UEM and TEM experiments were prepared by affixing crystals to Cu lift-out half grids (1 mm by 2 mm) with Ag epoxy and thinning with focused ion-beam (FIB) milling (Thermo Fisher/FEI Quanta 200 3D and Thermo Fisher/FEI Helios). A protective Pt layer (1.5 μm thick) was deposited from trimethyl(methylcyclopentadienyl) Pt(IV) precursor onto all FIB-prepared samples prior to milling. Final dimensions of the electron-transparent region of the specimens were generally 6.5

μm wide along the edge by 2.5 μm into the bulk, with thickness increasing approximately linearly from the free edge (40 nm at the edge to 120 nm at the 2.5-μm position). The electron-transparent region was surrounded on three sides by thicker, non-transparent material. Specimen thickness was mapped using electron energy-loss spectroscopy (EELS; Gatan Enfina) in a Thermo Fisher/FEI Tecnai G2 F30 operated at 300 kV in scanning mode with probe convergence and collection angles of 8.1 mrad and 10.4 mrad, respectively [50].

4D UEM measurements. All TEM and UEM imaging and diffraction measurements were conducted with a Thermo Fisher/FEI Tecnai Femto TEM operated at 200 kV. The electron source consisted of a truncated LaB_6 cathode (100-μm diameter) encircled with a graphite sheath for additional beam stabilization (Applied Physics Technologies) [51]. Images were acquired with a Gatan Orius SC200B 4-MP CCD camera with 14-bit dynamic range. A liquid nitrogen double-tilt specimen holder with Faraday cup and temperature controller (Gatan 636.MA) was used for all measurements at 300 K and at 100 K. Note that these temperatures were initial and therefore reference temperatures; finite element simulations were used to estimate maximum single-pulse photothermal temperature rises of the lattice to 321 K and 137 K, respectively [52].

A Yb:KGW diode-pumped solid-state laser (6 W, PHAROS, Light Conversion) was used to pump the specimen and to also generate the photoelectron packets by sending split pulses along two separate optical lines. At both temperatures, specimens were excited *in situ* with near-IR 1.2 eV photons, a pulse duration of 300 fs (fwhm; measured with a scanning autocorrelator; GECO, Light Conversion), a 50-kHz repetition rate, and an incident fluence of 3.6 mJ/cm^2 with calculated absorbed fluences of 0.62 mJ/cm^2 at 300 K and 0.63 mJ/cm^2 at 100 K (slight difference in calculated absorbed fluence due to temperature dependence of the LaFeAsO optical constants) [52-54]. Average laser power was measured externally with a power meter (Newport)

and extrapolated to the specimen position inside the UEM column by accounting for losses at optical elements. Simulations indicated specimen photothermal heating from a single pump pulse fully dissipated in less than 1 μs, well within the 20 μs pulse-to-pulse window [52]. The pump spot size was approximately 100 μm (fwhm), as estimated using a beam profiler (Newport) and extrapolation to the specimen plane. Photoexcitation was incident at 4° off normal relative to both the [*001*] crystallographic direction and to the incident electron wave vector, $\mathbf{k}_i$ (electron beam was assumed to be parallel). Fourth-harmonic light (4.8 eV) was generated using a harmonics module (HIRO, Light Conversion) and additional external non-linear optics. Photoelectron packet duration was estimated to be 1 ps (fwhm) based on estimated probe laser fluence, photon energy and estimated LaB_6 work function, and the position of the source relative to the Wehnelt aperture [51,55]. Time delay was controlled with a motorized linear translation stage (Aerotech PRO165LM with Soloist CP10-MXU controller) equipped with a broadband hollow retroreflector (Newport UBBR2.5-1UV). Time points were acquired in a randomized, non-sequential manner with various time steps *via* automated communication between the camera and the translation stage controller [43,56].

RESULTS AND DISCUSSION

A representative UEM selected-area bright-field image sequence of fs photoinduced structural dynamics in LaFeAsO at 300 K is shown in Figure 1. The specimens were single crystalline, as confirmed with selected-area electron diffraction (SAED), while the nanoscale to microscale morphology consisted generally of a freestanding wedge with an ill-defined and jagged apex created during FIB milling (Fig. 1a). Note that bright-field UEM images are generated in the same way as with conventional TEM. Briefly, the transmitted direct beam is

selected with an aperture to form the image, while all Bragg beams are blocked. In this way, dark image features correspond to specimen regions that are strongly scattering. Here, however, we found that photoinduced dynamics were more discernible when not using an aperture. This is because the thickness of the specimen generated strong scattering, thus obscuring the weaker transient diffraction contrast arising from ultrafast lattice distortions and the locally modulated Bragg condition [57].

Following *in situ* fs photoexcitation, two distinct responses occurring on different timescales were observed (Fig. 1b,c). It was found that the strongest, most discernable signals occurred in two distinct regions of interest (ROIs), though dynamics were generally observed across the entire crystal in the field of view (see Video S1). The first distinct response was most noticeable in ROI 1 and consisted of an initial spatial shift of image contrast occurring over the first ~30 ps following photoexcitation (Fig. 1b). The second response followed the first and was most noticeable in ROI 2. This second response began ~60 ps after photoexcitation, persisted for the duration of this particular experiment (out to t = 340 ps), and consisted of coherent propagating contrast plane waves moving from the wedge apex toward the bulk of the crystal (Fig. 1c). The coherent response in ROI 2 arises from the photoexcitation of CAPs [58-60], the behaviors and dynamics of which have been previously described for other materials within the context of UEM measurements [35,38,41,57]. At delay times beginning at t ~1 ns and extending to nearly 4 ns (limit of the experiment; not shown), the coherent contrast dynamics give way to complex, incoherent behavior arising from wave scattering and interference, similar to what has been observed with UEM in 1*T*-TaS_2 and 2*H*-MoS_2 [36,37].

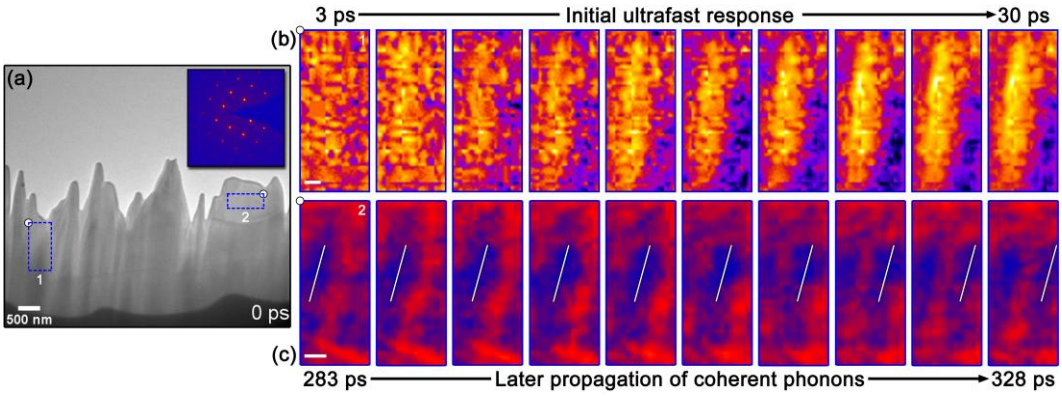

Figure 1. Initial precursor response and subsequent onset of CAPs in single-crystal LaFeAsO at 300 K. (a) Representative UEM image at t = 0 ps of a FIB-prepared specimen viewed approximately along the [*001*] direction (see the inset SAED pattern). Blue dashed rectangles (1 and 2) are select ROIs within which dynamics were imaged. White dots are orientation markers (see upper-left corners of the first frames in panels b and c). (b) Series of ROI-1 image-correlation maps generated with the *Image CorrelationJ 1o* plugin in ImageJ using the t = 0 ps frame as the source [61]. The series shows the initial onset of ultrafast dynamics spanning the first 30 ps after *in situ* fs photoexcitation. Changes in color temperature denote regions of diminishing correlation coefficient relative to the t = 0 ps frame. Scale bar = 100 nm. (c) Series of ROI-2 frames showing CAP propagation at later times following the precursor dynamics. White lines mark the approximate position and orientation of an individual phonon wavefront tracked across the series. Color gradient generated in Photoshop and was applied after making brightness and contrast adjustments to enhance the features of interest. Blue color denotes strong electron-scattering regions. Scale bar = 100 nm.

In order to quantify and to better understand the timescales and precise behaviors apparent in Video S1 and summarized in Figure 1, correlation and relative-intensity methods employing a source/reference frame were used (Fig. 2). The temporal response of the initial

ultrafast contrast shift observed in ROI 1 (Fig. 1a and with false coloring in Fig. 2a) was quantified by correlating the ROI in each frame in the Video S1 series to that of a source frame (t_s = -35 ps). This was done by using the *Image Correlator* plugin in ImageJ to determine a correlation coefficient (R) and then plotting this as a function of the time delay, t (Fig. 2b) [61]. The behavior of R *vs.* t for the initial dynamics displays a sigmoid response (Equation 1),

$$R = R_{min} + \frac{(R_{max} - R_{min})}{1 + e^{(t - t_{0.5})/dt}} \qquad (1)$$

with a reduction in R from 1.00 (correlating the t = -35 ps frame to itself) to below 0.90 spanning ~100 ps around time zero (t = 0 ps). Time zero is defined as the intersection of R_{max} with a tangent line at the inflection point, $t_{0.5}$. Following this, a fit value of $t_{0.5}$ = 17.8 ± 0.3 ps was found (error is the standard error of the fit). Further, an indicator of the timescale of the full initial response can be defined by determining the intersection point of R_{min} and the tangent line, thus mirroring the definition of t = 0 ps. In this way, the full initial response (*i.e.*, Δt for R_{max} to R_{min}) was found to be 35.6 ps for ROI 1.

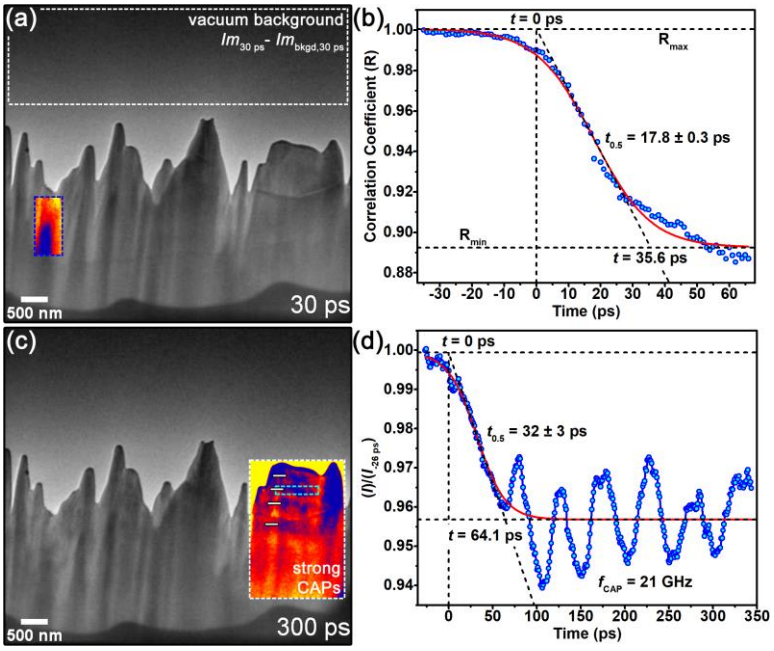

Figure 2. Timescales of discrete behaviors of fs photoinduced structural dynamics in LaFeAsO at 300 K. (a) Representative UEM image (t = 30 ps; Im_{30ps}) of the LaFeAsO specimen with vacuum background subtracted (bkgd, white dashed rectangle; $Im_{30ps} - Im_{bkgd,30ps}$) and brightness and contrast enhanced for presentation purposes only – analyses were done on unprocessed images. Blue dashed rectangle is ROI 1 in which image correlation was conducted. (b) Correlation coefficient (R) *vs.* time delay, t (1 ps steps), of ROI 1 in panel a. The best-fit of Equation 1 is shown in red. (c) Representative UEM image (t = 300 ps) processed the same as that in panel a. Light blue dashed rectangle is the ROI in which raw integrated intensity (I) was determined. White dashed rectangle highlights the region displaying strong CAP dynamics. Horizontal white dashes mark positions of individual CAP wavefronts. (d) Normalized raw integrated intensity $\left[\frac{(I)}{(I_{-26ps})}\right]$ *vs.* time delay, t (1 ps steps), of the region outlined by the light blue dashed rectangle in panel c. The best-fit of Equation 1 is shown in red. An FFT of the oscillatory signal beginning at t = 65 ps returned f_{CAP} = 21 GHz.

The specimen region displaying clear and strong CAP dynamics was quantified using raw integrated image intensities (I) (Fig. 2c,d) [35,38,41,57]. Coherent phonon dynamics were most apparent in this region owing to the wedge apex morphology, which consisted of a relatively extended, quasi-linear edge. Prior studies have found that morphologies of this type are well-suited to launch of discernable photoexcited CAPs propagating along a single wave vector, $\mathbf{k}_{CAP}$ [35,36,39]. (Note that false coloring was used to enhance the contrast from individual phonon wave fronts, which appear as dark-blue bands oriented parallel to the wedge edge.) Upon inspection of Video S1 one finds that, while coherent dynamics can be seen in other regions of the crystal, those particular behaviors are indicative of CAP generation from a point-like source,

of which there are several comprising the wedge edge. As such, the associated contrast dynamics were less amenable to quantitative analysis despite arising from the same basic mechanism as for the extended edge. The transient behavior within the ROI in Figure 2c (horizontal light blue dashed rectangle) was quantified by comparing I_t for each t to that at t = -26 ps (*i.e.*, by plotting $\frac{I}{I_{-26ps}}$ *vs. t*; Fig. 2d), again using ImageJ [61]. The overall behavior consisted of an initial sigmoid response as in ROI 1 (Equation 1 with R replaced by $\frac{I}{I_{-26ps}}$), but with a longer $t_{0.5}$ value of 32 ± 3 ps, followed by a coherent oscillation with frequency f_{CAP} = 21 GHz beginning ~60 ps after t = 0 ps. The lifetime of the oscillations is ~1 ns, significantly beyond the temporal window of the experiment (t_{max} = 340 ps).

The dynamics in Figure 2b,d spanning the first 30 to 60 ps prior to the onset of CAP oscillations for the T = 300 K specimen are attributed to photothermal expansion following fs photoexcitation. Using finite element modeling, a single pump pulse was estimated to transiently increase the lattice temperature by 21 K and displayed an initial sigmoid-like temporal response [52]. The initial shift in image contrast is attributed to anisotropic lattice expansion owing to the photoexcitation geometry (near normal incidence to the crystal surface), the optical penetration depth profile, and a resulting picometer-scale reorientation of the crystal that causes a change in local Bragg scattering conditions [57,62,63]. A shift to lower intensity in a particular specimen spot suggests enhanced alignment of a set of *hkl* Bragg planes in real-space with $\mathbf{k}_i$ such that stronger scattering occurs (and thus fewer electrons reach the detector). Therefore, the discrete spatiotemporal responses of contrast motion are a direct indicator of *local* timescales and reorientation dynamics. For a given material and photoexcitation condition, the timescales and dynamics of such motions are influenced not only by intrinsic properties but also by local structure, morphology, geometry, and boundary (initial) conditions. This, together with

convolution with spatially dependent CAP dynamics, explains the different $t_{0.5}$ values for the different ROIs at 300 K shown in Figure 2. Indeed, ps photothermal expansion is a precursor to CAP excitation and launch, as seen with side-peak formation and reductions in peak intensities in ultrafast diffraction experiments at high excitation fluences [23,64].

In undoped LaFeAsO, carrier and lattice thermalization is thought to occur during the first few picoseconds following fs photoexcitation; temperature-dependent relaxation of photoexcited quasiparticle dynamics span ~1 to 2 ps, as determined with ultrafast reflectivity measurements [48]. For that study, measurements were done out to t = 8 ps at various temperatures above and below the structural and magnetic phase transition points. Because of the dearth of non-equilibrium studies of LaFeAsO, we looked to other related materials to glean insight and to correlate to other signal responses. With ultrafast X-ray diffraction, the orthorhombic distortion in $BaFe_2As_2$ at low temperatures was found to be suppressed upon photoexcitation with 110 fs pulses of $h\nu$ = 1.5 eV photons and absorbed fluences up to 3.3 mJ/cm^2, with the order parameter decaying with a *fluence-independent* time constant of τ = 35 ps, much slower than suppression of the electron-ordering phases [18,23,65]. At elevated fluences, this response was convoluted with strain-wave excitation and launch spanning the first 25 ps. Additional suppression of the orthorhombic phase was also observed on much longer timescales (nanoseconds). The distinct initial suppression with τ = 35 ps was tentatively assigned to preferential atomic rearrangement at domain boundaries, where constraints imposed by the extended crystal lattice are relaxed; subsequent translations of atoms within the domain volume are coupled to acoustic phonons propagating at the longitudinal speed of sound (v_L ~6 nm/ps for $BaFe_2As_2$). Disparate timescales for quasiparticle and structural dynamics are indicative of separate trajectories followed by each degree of freedom, implying coupling

mechanisms are at work [23]. Indeed, nematic fluctuations are responsible for relatively long recoveries of tens of picoseconds of ultrafast optical ellipticity spanning a range of temperatures below the structural transition point in $BaFe_2As_2$ [65]. Though we are not claiming direct observation of any mechanisms of these types, the comparable timescales and structural responses are intriguing from an experimental accessibility point of view.

Prior to presenting the structural dynamics of the LaFeAsO specimen at 100 K, we provide a more in-depth analysis of the CAP behaviors at 300 K in order to establish baseline responses for correlating to phonon-driven atomic translations associated with the structural distortion [23]. Indeed, hypersonic phase velocities (v_p) of the first few phonon wavefronts for photoexcited dispersive modes supported by thin crystals (*i.e.*, plates) have potential implications for timescales of transformations nucleated at domain boundaries [23,38,41,42]. Accordingly, Figure 3 summarizes an in-depth analysis of the fs photoexcited CAP behavior observed within the highlighted ROI shown in Figure 2c (*i.e.*, the region showing strong CAP responses in Video S1). Note that the FIB milling process introduced a region of relatively abrupt but very small change in thickness delineated by a discrete terrace (white arrow in Figure 3a). This had no impact on the dynamics of interest and is noted simply for thoroughness. Photoexcited CAPs were observed emerging from the vacuum-crystal interface and propagating toward the bulk region across both sections along $\mathbf{k}_{CAP}$ approximately perpendicular to the free edge. Wavefront v_p was determined by fitting the associated contrast band with a Gaussian peak function and tracking the peak-center position over time (Fig. 3b,c). Seven measurable contrast bands were observed within the 340 ps experiment window (Fig. 3d).

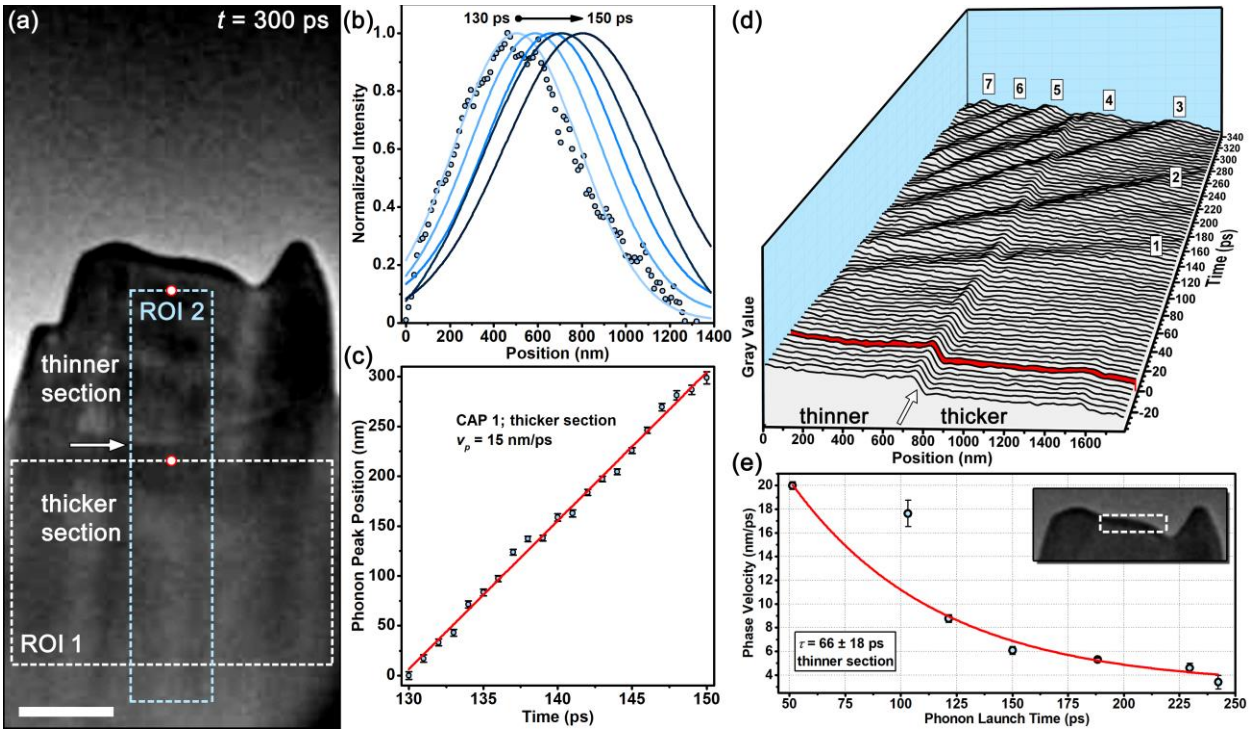

Figure 3. CAP velocities and dispersion behaviors in LaFeAsO at 300 K. (a) Representative UEM image of the specimen region. The image has been background adjusted for uneven electron-beam illumination, and the brightness and contrast have been enhanced to highlight key features. The horizontal arrow indicates the slight change in thickness introduced during FIB milling. Scale bar = 500 nm. (b) Select wavefront positions in ROI 1 (panel a) of the first photoexcited CAP. Solid curves are Gaussian best fits (data points shown only for the first peak for clarity). The 0-nm position is marked with a red-circled white dot in panel a. (c) Peak position *vs.* time of the first CAP wavefront in ROI 1. Error bars are standard errors of the fits. Red line is a linear least-squares fit. (d) Waterfall plot of 1D contrast profiles generated from ROI 2 (panel a), with the t = 0 ps profile shown in red for reference. Seven separate CAPs were observed in the 340 ps window. The static region delineating the thicker and thinner sections is indicated with an arrow. The 0-nm position is marked with a red-circled white dot in panel a. (e) Dispersion of v_p in the thinner section of ROI 2. Phonon launch time is defined as the

moment each CAP was launched from the region shown in the inset (white dashed rectangle). Red line is a single-exponential decay fit. Error is the standard error of the fit.

As shown in Figure 3, v_p of each individual photoexcited CAP is non-dispersive (*i.e.*, displays a constant v_p; Fig. 3c,d), while the overall wave train shows a dispersive behavior, relaxing from initially hypersonic values to the bulk speed of sound following a single exponential decay $\left(v_p = v_{p,0} + Ae^{-t_{launch}/\tau}\right)$ with time constant τ = 66 ± 18 ps (Fig. 3e). The fit returns a value $v_{p,0}$ = 3.1 ± 1.5 nm/ps for the extrapolated fully relaxed velocity. The fit errors are large mainly due to the single data point generated from the second contrast band falling well off the curve; this had minimal impact on the overall dispersive behavior as seen from the fit, and the origin may be due to a relatively poor fit (note the larger error bar). Similar UEM imaging measurements of CAP dispersion in Ge and GaAs single crystals also showed fully relaxed velocities matching the bulk speed of sound (~5 nm/ps) [38,41]. Here, 3.1 nm/ps is in good agreement with the calculated shear velocity in polycrystalline LaFeAsO (v_s = 2.9 nm/ps) but significantly differs from the longitudinal velocity (v_L = 5.09 nm/ps) [66,67]. This indicates the symmetry of the photoexcited mode is that of a shear (antisymmetric) propagating wave, which arises from the photoexcitation geometry and anisotropic initial photothermal expansion due to the optical penetration depth profile. Further, the dispersive behavior indicates the mode is of antisymmetric A_1 symmetry for thin crystal geometries; the A_0 mode is relatively non-dispersive, and higher-order modes occur at significantly higher frequencies than 21 GHz for the specimen geometry and material properties [45,52,68-70]. Note that the phonon launch time (t_{launch}) was calculated by extrapolating back to the crystal edge (white dashed rectangle in the Figure 3e inset). In this way, t_{launch} of the first wavefront was calculated to occur at t = 51 ps and

propagated along $\mathbf{k}_{CAP}$ with v_p = 20 nm/ps, in good agreement with the ~60 ps change in image intensity attributed to initial photothermal expansion (Fig. 2d).

The repeating light-dark banded contrast pattern arising from the CAP wave train (see Video S1, Fig. 2c, and Fig. 3a) indicates the *hk*0 diffracting planes (zone axis approximately along the [*001*] direction) are tilted back and forth in response to the coherent energy propagation, thus modulating the Bragg scattering condition [57]. Accordingly, each wavefront is comprised of a spatially varying strain profile along the direction parallel to $\mathbf{k}_i$ that matches the displacement field of the A_1 mode. At the unit cell level this produces an oscillating tensile and compressive strain oriented along the *ab* planes (*i.e.*, along the LaO and FeAs layers) [45]. This should produce a picoscale modulation of the La-La and Fe-Fe distances that translates into an oscillatory change in the La-O and Fe-As heights. It would therefore be interesting to measure this hypothesized CAP-induced height change and compare it to the amplitude of the fs photoexcited A_{1g} Raman mode (*e.g.*, ~1.2 pm/mJ·cm^{-2} for $BaFe_2As_2$) [20]. Note that the precise deformation of the La-O and Fe-As units will also depend upon the in-plane wave vector, $\mathbf{k}_{CAP}$ (*e.g.*, $\mathbf{k}_{CAP}$ parallel to [*100*] *vs*. [*110*]).

In order to illustrate how CAP dynamics could potentially be used to probe the structural and magnetic phase changes, and to correlate the observed dynamics to known timescales of the orthorhombic distortion and nematic fluctuations in related materials [20,23,65], we also conducted UEM imaging experiments at T = 100 K. This initial temperature is well below both the structural (160 K) and the antiferromagnetic ordering (145 K) transition temperatures for LaFeAsO [45]. Again, image correlation (R) and normalized raw integrated image intensity (I) *vs. t* were determined for different ROIs within a crystalline specimen oriented such that the [*001*] direction was approximately parallel to $\mathbf{k}_i$ (Fig. 4a-c). As was the case at 300 K, different

regions displayed different contrast dynamics, meaning certain ROIs were more amenable to elucidating either the initial precursor dynamics or the CAP responses (see Figs. 1 and 2). Note that in Figure 4a, the upper-right region of the image is vacuum background, and the specimen region in the field of view is freestanding. The image is also rotated for display purposes, thus producing the black triangular section in the upper-left corner.

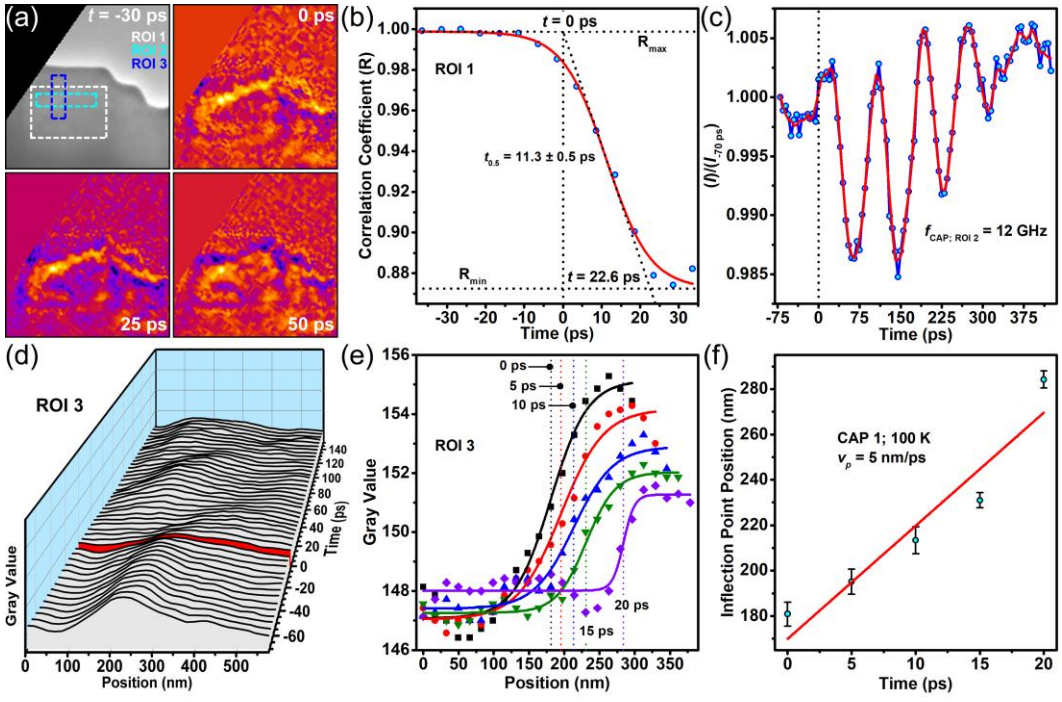

Figure 4. Photoinduced structural dynamics in LaFeAsO at T = 100 K. (a) Representative UEM image showing a select region of the specimen, along with image correlation maps at select times. Three ROIs are highlighted. Changes in color temperature relative to the cropped section denote regions of diminishing correlation relative to the t = -30 ps image. (b) Correlation coefficient (R) *vs.* t for ROI 1. The source was the t = -70 ps ROI (not shown). The best-fit of Equation 1 is shown in red. (c) Normalized raw integrated intensity $\left[\frac{(I)}{(I_{-70ps})}\right]$ *vs.* t for ROI 2. A smoothed line (solid red) is shown to guide the eye. An FFT of the oscillatory signal returned

f_{CAP} = 12 GHz. (d) Waterfall plot of 1D profiles generated from ROI 3, with the t = 0 ps profile shown in red for reference. Only two contrast bands were faintly observable in the 150 ps window after time zero. (e) Rising edge profiles of the first observable contrast band in ROI 3. Solid curves are sigmoid best fits, and the vertical dashed lines mark the $\left[\frac{(gray\ value)_{max}-(gray\ value)_{min}}{2}\right]$ positions. (f) Inflection points *vs.* t of the profiles in panel e. Error bars are the standard error of the sigmoid fits. Red line is a linear least-squares fit.

Both the photoinduced precursor timescale and the CAP behavior were noticeably different at 100 K. First, a shorter precursor timescale (*i.e.*, faster initial response) was observed, with $t_{0.5;100\ K}$ = 11.3 ± 0.5 ps and a full response of 22.6 ps (Fig. 4b). Second, for the ROI displaying observable CAP behavior (ROI 2, Fig. 4a,c), little to no precursor response was observed, and the frequency was reduced from $f_{CAP;300\ K}$ = 21 GHz to $f_{CAP;100\ K}$ = 12 GHz. Third, the CAP contrast strength was reduced relative to that at 300 K, suggesting that the phonon amplitudes may have been lower; this is further illustrated by the stronger CAP damping (*i.e.*, the shorter lifetime). Additionally, the observed weaker CAP response resulted in no observable dispersive behavior, perhaps due to a dearth of measurable wavefronts or due to weak excitation leading to generation of a different mode (Fig. 4d). Fourth and lastly, only a single v_p was measurable (Fig. 4e,f). Note that the t = 20 ps rising wavefront edge shown in Figure 4e (purple diamonds) was quite weak (only two points in the rising edge), and so the position was rather ill defined. Thus, the value for v_p from the fit to these five points is skewed upward (Fig. 4f). Accordingly, fitting only the t = 0 to 15 ps data returns v_p = 3.4 ± 0.1 nm/ps (not shown).

While some of the observed behaviors (*e.g.*, weaker CAP contrast and shorter overall relaxation time) may be attributed to a weaker photoinduced response (arising, for example, from

a weakening of electron-phonon interactions at lower temperatures [45]) or to the specific UEM imaging conditions, others (*e.g.*, the shorter precursor timescale and lower CAP frequency) are intriguingly correlated to changes in the static structural properties. Indeed, resonant ultrasound spectroscopic measurements of the elastic response of polycrystalline LaFeAsO specimens showed that a softening of the lattice, as per a reduction in the C_{11} and C_{44} elastic constants, occurs with cooling, reaching minimum values near ~140 K [45]. Here, this softening is positively correlated with the change in the values for f_{CAP}: 21 GHz at 321 K lowered to 12 GHz at 137 K (temperatures are simulated photothermal maximum values from initial reference temperatures of 300 K and 100 K, respectively [52]). Interestingly, such changes in the elastic properties are tied to nematic fluctuations through the shear modulus, C_{66}; because structural ordering is suggested to be induced by magnetic fluctuations, it stands to reason that variations in the strain-wave dynamics could also be correlated to the phase ordering [71]. We emphasize again, however, that this is simply a correlation; a number of morphological and geometrical factors can also produce variations in initial response and CAP frequency. While the objective here was to demonstrate the feasibility of conducting spatiotemporally-resolved studies of structural dynamics on Fe-pnictide materials with UEM, the observed differences are still intriguing and deserve further attention.

The absence of dispersive phase velocity behavior and the observation of a single v_p suggests a mostly non-dispersive zero-order mode was excited, either the symmetric S_0 or antisymmetric A_0 mode. The measured value of v_p = 3.4 nm/ps at $f_{CAP;100\ K}$ = 12 GHz is a better match to the S_0 mode (again, ignoring the data point at t = 20 ps; Fig. 4e,f [52]). The displacement field (symmetry) of this mode may also explain the weaker CAP contrast strengths and may have implications for Fe-As distortions, as with the shear A_1 mode seen at 300 K.

Excitation of different thin-crystal plate modes above and below the transition temperatures could occur from variations in specimen geometry, photoexcitation profile, elastic properties, or from magnetoelastic coupling strengths. It nevertheless is still intriguing to note that the faster precursor response in the ROI at lower temperature has hallmarks of nematic fluctuations competing with the photothermal lattice expansion [65]. Thus, in addition to demonstration of the sensitivity of UEM imaging measurements to local dynamics, the observations reported here suggest that CAP dynamics and associated transient propagating strains could potentially be used to probe nanoscale phase ordering and transitions in the Fe-pnictide materials. The measurements here being correlative, additional systematic UEM imaging or ultrafast convergent-beam electron diffraction studies [72] in the vicinity of the phase transition temperatures could aid in further elucidating the microscopic details and correlations while also avoiding sources of artifacts and confounding effects leading to challenges with interpretation [73].

CONCLUSIONS

We report the first study of the fs photoinduced structural dynamics of undoped LaFeAsO above and below the structural and antiferromagnetic ordering transition temperatures using 4D ultrafast electron microscopy (UEM). With nanometer-ps UEM imaging, we have shown that variations in transient lattice responses and coherent acoustic phonon dynamics are intriguingly correlated with nematic fluctuations near the transition temperature and with the elastic properties of the two structural phases. The correlated behaviors manifest in precursor timescales and through various CAP behaviors that include frequency, dispersion, phase velocity, and mode symmetry. Further, specimen geometry and boundary conditions were

shown to influence the *local* nature of the photoinduced strain waves, thus suggesting a potential pathway to directing responses and thus producing spatially separated transient states. Overall, these experiments illustrate a new way of potentially probing the coupling of degrees of freedom and the interconnected structural and magnetic orders with high real-space spatiotemporal resolution once confounding factors are accounted for and controlled.

Acknowledgments: This material is based upon work supported primarily by the U.S. Department of Energy, Office of Science, Office of Basic Energy Sciences under Award No. DE-SC0018204. This work was supported partially by the National Science Foundation through the University of Minnesota MRSEC under Award Number DMR-2011401 and partially by the U.S. Department of Energy through the UMN Center for Quantum Materials under Grant No. DE-SC-0016371. Partial funding provided by the Arnold and Mabel Beckman Foundation in the form of a Beckman Young Investigator Award. The LaFeAsO crystals were synthesized and provided by Jiaqiang Yan and David Mandrus. We acknowledge a helpful discussion with Rafael Fernandes about differences in the structural dynamics and correlation to ordering and phase behavior.

Author Contributions: R.A.G. contributions were formal analysis, investigation, validation, visualization, and writing – original draft. P.K.S. contributions were formal analysis, investigation, validation, visualization, and writing – original draft. J.C. contributions were formal analysis and visualization. D.J.F. contributions were conceptualization, formal analysis, funding acquisition, methodology, project administration, resources, supervision, visualization,

writing – original draft, and writing – review and editing. See the NISO CRediT taxonomy for definitions of contributing roles (credit.niso.org).

Conflicts of interest: The authors declare no competing interests.

*Author to whom correspondence should be addressed.

Email: flan0076@umn.edu

Office: +1 612-625-3867

Supplemental Material: The Supplemental Material contains Supporting Video S1 and caption of UEM imaging of LaFeAsO dynamics at 300 K, additional methods describing calculation of the absorbed fluence, finite element simulations of the transient photothermal response, calculation of the CAP phase velocity dispersion curves for LaFeAsO, Figure S1 showing the transient photothermal responses at each initial temperature, and Figure S2 showing the calculated dispersion curves.

References

[1] N. Gedik, D.-S. Yang, G. Logvenov, I. Bozovic, and A. H. Zewail, Science **316**, 425 (2007).

[2] F. Carbone, D.-S. Yang, E. Giannini, and A. H. Zewail, Proc. Natl. Acad. Sci. U.S.A. **105**, 20161 (2008).

[3] A. Pashkin, M. Porer, M. Beyer, K. W. Kim, A. Dubroka, C. Bernhard, X. Yao, Y. Dagan, R. Hackl, A. Erb, J. Demsar, R. Huber, and A. Leitenstorfer, Phys. Rev. Lett. **105**, 067001 (2010).

[4] B. Mansart, M. J. G. Cottet, G. F. Mancini, T. Jarlborg, S. B. Dugdale, S. L. Johnson, S. O. Mariager, C. J. Milne, P. Beaud, S. Grübel, J. A. Johnson, T. Kubacka, G. Ingold, K.

Prsa, H. M. Rønnow, K. Conder, E. Pomjakushina, M. Chergui, and F. Carbone, Phys. Rev. B **88**, 054507 (2013).

[5] R. Mankowsky, A. Subedi, M. Först, S. O. Mariager, M. Chollet, H. T. Lemke, J. S. Robinson, J. M. Glownia, M. P. Minitti, A. Frano, M. Fechner, N. A. Spaldin, T. Loew, B. Keimer, A. Georges, and A. Cavalleri, Nature **516**, 71 (2014).

[6] M. Först, R. I. Tobey, H. Bromberger, S. B. Wilkins, V. Khanna, A. D. Caviglia, Y. D. Chuang, W. S. Lee, W. F. Schlotter, J. J. Turner, M. P. Minitti, O. Krupin, Z. J. Xu, J. S. Wen, G. D. Gu, S. S. Dhesi, A. Cavalleri, and J. P. Hill, Phys. Rev. Lett. **112**, 157002 (2014).

[7] M. Först, A. Frano, S. Kaiser, R. Mankowsky, C. R. Hunt, J. J. Turner, G. L. Dakovski, M. P. Minitti, J. Robinson, T. Loew, M. Le Tacon, B. Keimer, J. P. Hill, A. Cavalleri, and S. S. Dhesi, Phys. Rev. B **90**, 184514 (2014).

[8] V. Khanna, R. Mankowsky, M. Petrich, H. Bromberger, S. A. Cavill, E. Möhr-Vorobeva, D. Nicoletti, Y. Laplace, G. D. Gu, J. P. Hill, M. Först, A. Cavalleri, and S. S. Dhesi, Phys. Rev. B **93**, 224522 (2016).

[9] R. Mankowsky, M. Fechner, M. Först, A. v. Hoegen, J. Porras, T. Loew, G. L. Dakovski, M. Seaberg, S. Möller, G. Coslovich, B. Keimer, S. S. Dhesi, and A. Cavalleri, Struct. Dyn. **4**, 044007 (2017).

[10] S. Gerber, S.-L. Yang, D. Zhu, H. Soifer, J. A. Sobota, S. Rebec, J. J. Lee, T. Jia, B. Moritz, C. Jia, A. Gauthier, Y. Li, D. Leuenberger, Y. Zhang, L. Chaix, W. Li, H. Jang, J.-S. Lee, M. Yi, G. L. Dakovski, S. Song, J. M. Glownia, S. Nelson, K. W. Kim, Y.-D. Chuang, Z. Hussain, R. G. Moore, T. P. Devereaux, W.-S. Lee, P. S. Kirchmann, and Z.-X. Shen, Science **357**, 71 (2017).

[11] F. Novelli, G. Giovannetti, A. Avella, F. Cilento, L. Patthey, M. Radovic, M. Capone, F. Parmigiani, and D. Fausti, Phys. Rev. B **95**, 174524 (2017).

[12] T. Konstantinova, J. D. Rameau, A. H. Reid, O. Abdurazakov, L. Wu, R. Li, X. Shen, G. Gu, Y. Huang, L. Rettig, I. Avigo, M. Ligges, J. K. Freericks, A. F. Kemper, H. A. Dürr, U. Bovensiepen, P. D. Johnson, X. Wang, and Y. Zhu, Sci. Adv. **4**, eaap7427 (2018).

[13] M. Buzzi, M. Först, R. Mankowsky, and A. Cavalleri, Nat. Rev. Mater. **3**, 299 (2018).

[14] S. L. Yang, J. A. Sobota, Y. He, D. Leuenberger, H. Soifer, H. Eisaki, P. S. Kirchmann, and Z. X. Shen, Phys. Rev. Lett. **122**, 176403 (2019).

[15] M. Mitrano, S. Lee, A. A. Husain, M. Zhu, G. d. l. P. Munoz, S. X. L. Sun, Y. I. Joe, A. H. Reid, S. F. Wandel, G. Coslovich, W. Schlotter, T. van Driel, J. Schneeloch, G. D. Gu, N. Goldenfeld, and P. Abbamonte, Phys. Rev. B **100**, 205125 (2019).

[16] M. Mitrano, S. Lee, A. A. Husain, L. Delacretaz, M. H. Zhu, G. D. Munoz, S. X. L. Sun, Y. I. Joe, A. H. Reid, S. F. Wandel, G. Coslovich, W. Schlotter, T. van Driel, J.

Schneeloch, G. D. Gu, S. Hartnoll, N. Goldenfeld, and P. Abbamonte, Sci. Adv. **5**, eaax3346 (2019).

[17] T. Konstantinova, L. Wu, M. Abeykoon, R. J. Koch, A. F. Wang, R. K. Li, X. Shen, J. Li, J. Tao, I. A. Zaliznyak, C. Petrovic, S. J. L. Billinge, X. J. Wang, E. S. Bozin, and Y. Zhu, Phys. Rev. B **99**, 180102 (2019).

[18] K. W. Kim, A. Pashkin, H. Schäfer, M. Beyer, M. Porer, T. Wolf, C. Bernhard, J. Demsar, R. Huber, and A. Leitenstorfer, Nat. Mater. **11**, 497 (2012).

[19] L. X. Yang, G. Rohde, T. Rohwer, A. Stange, K. Hanff, C. Sohrt, L. Rettig, R. Cortés, F. Chen, D. L. Feng, T. Wolf, B. Kamble, I. Eremin, T. Popmintchev, M. M. Murnane, H. C. Kapteyn, L. Kipp, J. Fink, M. Bauer, U. Bovensiepen, and K. Rossnagel, Phys. Rev. Lett. **112**, 207001 (2014).

[20] L. Rettig, S. O. Mariager, A. Ferrer, S. Grubel, J. A. Johnson, J. Rittmann, T. Wolf, S. L. Johnson, G. Ingold, P. Beaud, and U. Staub, Phys. Rev. Lett. **114**, 067402 (2015).

[21] S. Gerber, K. W. Kim, Y. Zhang, D. Zhu, N. Plonka, M. Yi, G. L. Dakovski, D. Leuenberger, P. S. Kirchmann, R. G. Moore, M. Chollet, J. M. Glownia, Y. Feng, J. S. Lee, A. Mehta, A. F. Kemper, T. Wolf, Y. D. Chuang, Z. Hussain, C. C. Kao, B. Moritz, Z. X. Shen, T. P. Devereaux, and W. S. Lee, Nat. Commun. **6**, 7377 (2015).

[22] D. Parshall, L. Pintschovius, J. L. Niedziela, J. P. Castellan, D. Lamago, R. Mittal, T. Wolf, and D. Reznik, Phys. Rev. B **91**, 134426, 134426 (2015).

[23] L. Rettig, S. O. Mariager, A. Ferrer, S. Grubel, J. A. Johnson, J. Rittmann, T. Wolf, S. L. Johnson, G. Ingold, P. Beaud, and U. Staub, Struct. Dyn. **3**, 023611 (2016).

[24] T. Suzuki, Y. Kubota, A. Nakamura, T. Shimojima, K. Takubo, S. Ito, K. Yamamoto, S. Michimae, H. Sato, H. Hiramatsu, H. Hosono, T. Togashi, M. Yabashi, H. Wadati, I. Matsuda, S. Shin, and K. Okazaki, Phys. Rev. Res. **3**, 033222 (2021).

[25] D. H. Torchinsky, J. W. McIver, D. Hsieh, G. F. Chen, J. L. Luo, N. L. Wang, and N. Gedik, Phys. Rev. B **84**, 104518 (2011).

[26] S. Kumar, L. Harnagea, S. Wurmehl, B. Buchner, and A. K. Sood, EPL **100**, 57007, 57007 (2012).

[27] S. Kumar, L. Harnagea, S. Wurmehl, B. Buchner, and A. K. Sood, J. Phys. Soc. Jpn. **82**, 044715 (2013).

[28] K. H. Lin, K. J. Wang, C. C. Chang, Y. C. Wen, B. Lv, C. W. Chu, and M. K. Wu, Sci. Rep. **6**, 25962 (2016).

[29] D. Cheng, B. Song, J. H. Kang, C. Sundahl, L. Luo, J.-M. Park, Y. G. Collantes, E. E. Hellstrom, M. Mootz, I. E. Perakis, C. B. Eom, and J. Wang, arXiv:2110.09728 (2021).

[30] N. Takeshita, T. Sasagawa, T. Sugioka, Y. Tokura, and H. Takagi, J. Phys. Soc. Jpn. **73**, 1123 (2004).

[31] S. Medvedev, T. M. McQueen, I. A. Troyan, T. Palasyuk, M. I. Eremets, R. J. Cava, S. Naghavi, F. Casper, V. Ksenofontov, G. Wortmann, and C. Felser, Nat. Mater. **8**, 630 (2009).

[32] J. H. Chu, H. H. Kuo, J. G. Analytis, and I. R. Fisher, Science **337**, 710 (2012).

[33] Z. Guguchia, D. Das, C. N. Wang, T. Adachi, N. Kitajima, M. Elender, F. Brückner, S. Ghosh, V. Grinenko, T. Shiroka, M. Müller, C. Mudry, C. Baines, M. Bartkowiak, Y. Koike, A. Amato, J. M. Tranquada, H. H. Klauss, C. W. Hicks, and H. Luetkens, Phys. Rev. Lett. **125**, 097005 (2020).

[34] T. Worasaran, M. S. Ikeda, J. C. Palmstrom, J. A. W. Straquadine, S. A. Kivelson, and I. R. Fisher, Science **372**, 973 (2021).

[35] D. R. Cremons, D. A. Plemmons, and D. J. Flannigan, Nat. Commun. **7**, 11230 (2016).

[36] D. R. Cremons, D. A. Plemmons, and D. J. Flannigan, Struct. Dyn. **4**, 044019 (2017).

[37] A. J. McKenna, J. K. Eliason, and D. J. Flannigan, Nano Lett. **17**, 3952 (2017).

[38] D. R. Cremons, D. X. Du, and D. J. Flannigan, Phys. Rev. Mater. **1**, 073801 (2017).

[39] Y. Zhang and D. J. Flannigan, Nano Lett. **19**, 8216 (2019).

[40] S. A. Reisbick, Y. Zhang, and D. J. Flannigan, J. Phys. Chem. A **124**, 1877 (2020).

[41] E. J. VandenBussche and D. J. Flannigan, Philos. Trans. R. Soc. London A **378**, 20190598 (2020).

[42] S. A. Reisbick, Y. Zhang, J. Chen, P. E. Engen, and D. J. Flannigan, J. Phys. Chem. Lett. **12**, 6439 (2021).

[43] Y. Zhang and D. J. Flannigan, Nano Lett. **21**, 7332 (2021).

[44] Y. Kamihara, T. Watanabe, M. Hirano, and H. Hosono, J. Am. Chem. Soc. **130**, 3296 (2008).

[45] M. A. McGuire, A. D. Christianson, A. S. Sefat, B. C. Sales, M. D. Lumsden, R. Jin, E. A. Payzant, D. Mandrus, Y. Luan, V. Keppens, V. Varadarajan, J. W. Brill, R. P. Hermann, M. T. Sougrati, F. Grandjean, and G. J. Long, Phys. Rev. B **78**, 094517 (2008).

[46] C. de la Cruz, Q. Huang, J. W. Lynn, J. Li, W. R. Ii, J. L. Zarestky, H. A. Mook, G. F. Chen, J. L. Luo, N. L. Wang, and P. Dai, Nature **453**, 899 (2008).

[47] J. Dong, H. J. Zhang, G. Xu, Z. Li, G. Li, W. Z. Hu, D. Wu, G. F. Chen, X. Dai, J. L. Luo, Z. Fang, and N. L. Wang, EPL **83**, 27006 (2008).

[48] R. Chen, T. Dong, H. Wang, and N. Wang, Sci. China: Phys., Mech. Astron. **56**, 2395 (2013).

[49] J. Q. Yan, S. Nandi, J. L. Zarestky, W. Tian, A. Kreyssig, B. Jensen, A. Kracher, K. W. Dennis, R. J. McQueeney, A. I. Goldman, R. W. McCallum, and T. A. Lograsso, Appl. Phys. Lett. **95**, 222504 (2009).

[50] R. F. Egerton and S. C. Cheng, Ultramicroscopy **21**, 231 (1987).

[51] D. A. Plemmons and D. J. Flannigan, Chem. Phys. Lett. **683**, 186 (2017).

[52] See Supplemental Material at [*URL will be inserted by publisher*] for additional methods, calculations, and simulations.

[53] A. V. Boris, N. N. Kovaleva, S. S. A. Seo, J. S. Kim, P. Popovich, Y. Matiks, R. K. Kremer, and B. Keimer, Phys. Rev. Lett. **102**, 027001 (2009).

[54] Z. G. Chen, R. H. Yuan, T. Dong, and N. L. Wang, Phys. Rev. B **81**, 100502 (2010).

[55] W. A. Curtis and D. Flannigan, Phys. Chem. Chem. Phys. **23**, 23544 (2021).

[56] D. X. Du, S. A. Reisbick, and D. J. Flannigan, Ultramicroscopy **223**, 113235 (2021).

[57] D. X. Du and D. J. Flannigan, Struct. Dyn. **7**, 024103 (2020).

[58] C. Thomsen, J. Strait, Z. Vardeny, H. J. Maris, J. Tauc, and J. J. Hauser, Phys. Rev. Lett. **53**, 989 (1984).

[59] H. J. Zeiger, J. Vidal, T. K. Cheng, E. P. Ippen, G. Dresselhaus, and M. S. Dresselhaus, Phys. Rev. B **45**, 768 (1992).

[60] P. Ruello and V. E. Gusev, Ultrasonics **56**, 21 (2015).

[61] C. A. Schneider, W. S. Rasband, and K. W. Eliceiri, Nat. Methods **9**, 671 (2012).

[62] B. Barwick, H. S. Park, O.-H. Kwon, J. S. Baskin, and A. H. Zewail, Science **322**, 1227 (2008).

[63] H. S. Park, J. S. Baskin, B. Barwick, O.-H. Kwon, and A. H. Zewail, Ultramicroscopy **110**, 7 (2009).

[64] C. Rose-Petruck, R. Jimenez, T. Guo, A. Cavalleri, C. W. Siders, F. Rksi, J. A. Squier, B. C. Walker, K. R. Wilson, and C. P. J. Barty, Nature **398**, 310 (1999).

[65] A. Patz, T. Li, S. Ran, R. M. Fernandes, J. Schmalian, S. L. Bud'ko, P. C. Canfield, I. E. Perakis, and J. Wang, Nat. Commun. **5**, 3229 (2014).

[66] I. R. Shein and A. L. Ivanovskii, Tech. Phys. Lett. **35**, 961 (2009).

[67] R. Abd-Shukor, J. Supercond. Novel Magn. **23**, 1229 (2010).

[68] H. Lamb, Proc. R. Soc. A **93**, 114 (1917).

[69] J. D. Achenbach, *Wave Propagation in Elastic Solids* (North-Holland Publishing Company, New York, 1973), 1 edn., Vol. 16.

[70] K. Brugger, J. Appl. Phys. **36**, 759 (1965).

[71] R. M. Fernandes, L. H. VanBebber, S. Bhattacharya, P. Chandra, V. Keppens, D. Mandrus, M. A. McGuire, B. C. Sales, A. S. Sefat, and J. Schmalian, Phys. Rev. Lett. **105**, 157003 (2010).

[72] A. Yurtsever and A. H. Zewail, Science **326**, 708 (2009).

[73] P. K. Suri, J. Yan, D. G. Mandrus, and D. J. Flannigan, J. Phys. Chem. C **120**, 18931 (2016).